

PUBLISHED VERSION

Francois, Alexandre; Rowland, Kristopher John; Afshar Vahid, Shahraam; Henderson, Matthew Ryan; Monro, Tanya Mary

Enhancing the radiation efficiency of dye doped whispering gallery mode microresonators, *Optics Express*, 2013; 21(19):22566-22577.

© 2013 Optical Society of America

PERMISSIONS

<http://www.opticsinfobase.org/submit/forms/copyxfer.pdf>

This paper was published in Optics Express and is made available as an electronic reprint with the permission of OSA. The paper can be found at the following URL on the OSA website

<http://www.opticsinfobase.org/oe/abstract.cfm?uri=oe-21-19-22566>

OSA grants to the Author(s) (or their employers, in the case of works made for hire) the following rights:

- (a) The right, after publication by OSA, to use all or part of the Work without revision or modification, including the OSAformatted version, in personal compilations or other publications consisting solely of the Author(s)' own works, including the Author(s)' personal web home page, and to make copies of all or part of the Work for the Author(s)' use for lecture or classroom purposes;
- (b) The right to post and update his or her Work on any internet site (other than the Author(s)' personal web home page) provided that the following conditions are met: (i) access to the server does not depend on payment for access, subscription or membership fees; and (ii) any such posting made or updated after acceptance of the Work for publication includes and prominently displays the correct bibliographic data and an OSA copyright notice (e.g. "© 2009 The Optical Society")..

4th December 2013

<http://hdl.handle.net/2440/81358>

Enhancing the radiation efficiency of dye doped whispering gallery mode microresonators

Alexandre François,* Kristopher J. Rowland, Shakraam Afshar V.,
Matthew R. Henderson, and Tanya M. Monro

*Institute for Photonics and Advanced Sensing (IPAS) and School of Chemistry and Physics, The University of
Adelaide, Adelaide SA 5005, Australia*

*alexandre.francois@adelaide.edu.au

Abstract: We present a novel form of a Whispering Gallery Mode (WGM) sensor that exploits dye doped polystyrene microspheres, as active resonators, positioned onto the tip of a Microstructured Optical Fiber (MOF) as a means of overcoming the limited Q-factors for small resonators. We show that it is possible to substantially enhance the fluorescence emission of selected WGMs of the microspheres, resulting in an increase of the signal-to-noise ratio of the modes and of the effective Q-factor. This is done by positioning the resonator into one of the holes of a suspended core MOF and matching the resonator diameter with the hole diameter where it sits, effectively breaking the symmetry of the environment surrounding the sphere. Furthermore we demonstrate that using this experimental configuration, the lasing efficiency of the dye-doped microspheres is also significantly enhanced, which also contributes to an enhancement in the observed Q-factor.

©2013 Optical Society of America

OCIS codes: (140.3945) Microcavities; (060.4005) Microstructured fibers; (280.4788) Optical sensing and sensors.

References and links

1. A. M. Armani, R. P. Kulkarni, S. E. Fraser, R. C. Flagan, and K. J. Vahala, "Label-Free, Single-Molecule Detection with Optical Microcavities," *Science* **317**(5839), 783–787 (2007).
2. I. M. White, H. Oveys, and X. Fan, "Liquid-core optical ring-resonator sensors," *Opt. Lett.* **31**(9), 1319–1321 (2006).
3. S. Arnold, M. Khoshshima, I. Teraoka, S. Holler, and F. Vollmer, "Shift of whispering-gallery modes in microspheres by protein adsorption," *Opt. Lett.* **28**(4), 272–274 (2003).
4. A. N. Oraevsky, "Whispering-gallery waves," *Quantum Electron.* **32**(5), 377–400 (2002).
5. A. B. Matsko and V. S. Ilchenko, "Optical Resonators With Whispering Gallery Modes – Part I: Basics," *IEEE J. Sel. Top. Quantum Electron.* **12**(1), 3–14 (2006).
6. V. S. Ilchenko and A. B. Matsko, "Optical Resonators With Whispering Gallery Modes – Part II: Applications," *IEEE J. Sel. Top. Quantum Electron.* **12**(1), 15–32 (2006).
7. E. Nuhiji and P. Mulvaney, "Detection of Unlabeled Oligonucleotide Targets Using Whispering Gallery Modes in Single, Fluorescent Microspheres," *Small* **3**(8), 1408–1414 (2007).
8. M. Himmelhaus, S. Krishnamoorthy, and A. François, "Optical Sensors Based on Whispering Gallery Modes in Fluorescent Microbeads: Response to Specific Interactions," *Sensors (Basel)* **10**(6), 6257–6274 (2010).
9. T. J. Kippenberg, S. M. Spillane, and K. J. Vahala, "Demonstration of ultra-high-Q small mode volume toroid microcavities on a chip," *Appl. Phys. Lett.* **85**(25), 6113 (2004).
10. P. Bianucci, J. R. Rodríguez, C. Clements, C. M. Hessel, J. G. C. Veinot, and A. Meldrum, "Whispering gallery modes in silicon nanocrystal coated microcavities," *Phys. Status Solidi, A Appl. Res.* **206**(5), 973–975 (2009).
11. K. J. Rowland, A. François, P. Hoffmann, and T. M. Monro, "Fluorescent polymer coated capillaries as optofluidic refractometric sensors," *Opt. Express* **21**(9), 11492–11505 (2013).
12. F. Vollmer and S. Arnold, "Whispering-gallery-mode biosensing: label-free detection down to single molecules," *Nat. Methods* **5**(7), 591–596 (2008).
13. H. T. Beier, G. L. Côté, and K. E. Meissner, "Modeling whispering gallery modes in quantum dot embedded polystyrene microspheres," *J. Opt. Soc. Am. B* **27**(3), 536–543 (2010).
14. V. R. Dantham, S. Holler, Z. Wan, V. Kolchenko, and S. Arnold, "Taking whispering gallery-mode single virus detection and sizing to the limit," *Appl. Phys. Lett.* **101**(4), 043704 (2012).

15. W. Tan, L. Shi, and X. Chen, "Modeling of an Optical Sensor Based on Whispering Gallery Modes (WGMs) on the Surface Guiding Layer of Glass Filaments," *Sensors (Basel Switzerland)* **8**(10), 6761–6768 (2008).
16. J. L. Nadeau, V. S. Ilchenko, D. Kossakovski, G. H. Bearman, and L. Maleki, "High-Q whispering-gallery mode sensor in liquids," *Proc. SPIE 4629, Laser Resonators and Beam Control V*, 172–180 (2002).
17. A. François and M. Himmelhaus, "Whispering gallery mode biosensor operated in the stimulated emission regime," *Appl. Phys. Lett.* **94**(3), 031101 (2009).
18. A. François, K. J. Rowland, and T. M. Monro, "Highly efficient excitation and detection of whispering gallery modes in a dye-doped microsphere using a microstructured optical fiber," *Appl. Phys. Lett.* **99**(14), 141111 (2011).
19. K. Kosma, G. Zito, K. Schuster, and S. Pissadakis, "Whispering gallery mode microsphere resonator integrated inside a microstructured optical fiber," *Opt. Lett.* **38**(8), 1301–1303 (2013).
20. D. E. Gómez, I. Pastoriza-Santos, and P. Mulvaney, "Tunable Whispering Gallery Mode Emission from Quantum-Dot-Doped Microspheres," *Small* **1**(2), 238–241 (2005).
21. G. Schneider, G. Decher, N. Nerambourg, R. Praho, M. H. V. Werts, and M. Blanchard-Desce, "Distance-dependent fluorescence quenching on gold nanoparticles ensheathed with layer-by-layer assembled polyelectrolytes," *Nano Lett.* **6**(3), 530–536 (2006).
22. I. T. S. Li and G. C. Walker, "Interfacial Free Energy Governs Single Polystyrene Chain Collapse in Water and Aqueous Solutions," *JACS* **132**(18), 6530–6540 (2010).
23. K. Klier, J. H. Shen, and A. C. Zettlemoyer, "Water on Silica and Silicate Surfaces. I. Partially Hydrophobic Silicas," *J. Phys. Chem.* **77**(11), 1458–1465 (1973).
24. M. Kuwata-Gonokami, K. Takeda, H. Yasuda, and K. Ema, "Laser Emission from Dye-Doped Polystyrene Microsphere," *Jpn. J. Appl. Phys.* **31**(Part 2, No. 2A), 99–101 (1992).
25. A. François and M. Himmelhaus, "Optical Sensors Based on Whispering Gallery Modes in Fluorescent Microbeads: Size Dependence and Influence of Substrate," *Sensors (Basel)* **9**(9), 6836–6852 (2009).
26. J. Zhang, J. Liu, S. Wang, P. Zhan, Z. Wang, and N. Ming, "Facile Methods to Coat Polystyrene and Silica Colloids with Metal," *Adv. Funct. Mater.* **14**(11), 1089–1096 (2004).
27. L. Yang, D. K. Armani, and K. J. Vahala, "Fiber-coupled erbium microlasers on a chip," *Appl. Phys. Lett.* **83**(5), 825 (2003).
28. A. F. Oskooi, D. Roundy, M. Ibanescu, P. Bermel, J. D. Joannopoulos, and S. G. Johnson, "Meep: A flexible free-software package for electromagnetic simulations by the FDTD method," *Comput. Phys. Commun.* **181**(3), 687–702 (2010).
29. I. M. White and X. Fan, "On the performance quantification of resonant refractive index sensors," *Opt. Express* **16**(2), 1020–1028 (2008).

1. Introduction

Whispering Gallery Modes (WGMs) are a resonance phenomenon that can occur in objects with at least one axis of revolution [1–6]. WGMs can be described as light trapped within a resonator by total internal reflection, circulating along the inner surface and returning in phase after a single or multiple round trips, and in this way satisfying resonance conditions [4,5]. The spectral position of these resonances is dictated not only by the resonator geometry (diameter and sphericity) and optical properties, but also by the environmental conditions (e.g. refractive index) in the vicinity of the resonator [4,5]. While resonators with different geometry and optical properties have been investigated [6], spheres [3,5,7,8], toroids [1,9] or capillaries [2,10,11] have been the most widely studied. Although these resonators exhibit useful properties, and have been widely used for refractive index sensing applications, substantial effort has been made in recent years to improve their sensing performance. Researchers have moved towards using smaller resonators, with early work considering sub-millimeter [3,12] silica spheres, and more recent developments enabling resonators as small as 10 to 50 μm in diameter [7,8,13,14]. Note that the refractive index sensitivity ($S = \delta\lambda/\delta n$) is known to be inversely proportional to the resonator radius ($\Delta\lambda/\lambda = \Delta R/R$) [3,15]. Reducing the diameter of the resonator has one substantial drawback; namely that the resolution of the sensor, which is related to the Q-factor of the resonator, decreases significantly for small resonators. Large resonators, ranging from 50 to 300 μm in diameter, typically exhibit a Q-factor up to several millions [1,3,16], whereas smaller resonators (below 20 μm in diameter) reported in literature have been limited to a Q-factor of around 10^3 in liquids [8,13]. One approach for improving the Q-factor of small resonators is the use of active resonators [6,7,17] which contain a gain medium (unlike passive resonators [1–3]) and can induce lasing of the WGMs. Using this strategy, it has been found that the Q-factor of the lasing modes can

be increased by up to a factor 5, compared to the non-lasing modes, as the signal-to-noise ratio is significantly increased [17].

Recently we demonstrated that a dye-doped microresonator positioned onto the tip of a suspended core Microstructured Optical Fiber (MOF) can be used as a dip sensor [18]. In this architecture, the resonator is located on a circular air hole next to the fiber core, enabling a significant portion of the sphere to overlap with the guided light emerging from the cleaved fiber tip [18]. When the resonator is excited through the suspended core fiber, it exhibits an unusually high radiative efficiency, which was initially attributed simply to the higher excitation efficiency that this architecture enables. More recently, Kosma et al. have published an article describing the use of a single polystyrene microsphere directly embedded within a similar MOF for sensing purposes [19]. While trying to use a similar concept, their excitation scheme, using a passive resonator and looking at the scattering from the resonator at 90 degrees, did not allow them to observe any effect produced by the microstructured optical fiber environment on the performance of the resonator. Here, we further investigate the enhancement of the resonator emission when it is positioned onto the MOF tip. We use a new configuration, which rules out the attribution of higher radiation efficiency to higher excitation efficiency. Instead, we show that high radiative efficiency is purely due to the change of the surrounding geometry of the microresonators, which results in selectively enhancement of some WGM-based radiation peaks. The impact of the radiative enhancement on the WGM lasing threshold for different configurations is explored, and the consequences of this enhancement on the sensor's Quality factor evaluated. Finally we show that this phenomenon can be exploited for generating WGM spectra in smaller microspheres, to exploit their higher refractive index sensitivity [3,15].

2. Materials and methods

2.1 Materials

Polystyrene (PS) microspheres ($n_{\text{PS}} = 1.59$) were purchased from Polysciences, Inc., Warrington. Nile red fluorescent dye and xylene were received from Sigma-Aldrich, all chemicals were used as received.

2.2 Microsphere preparation

Polystyrene microspheres with a nominal diameter of 5 μm , 15 μm , 20 μm and 25 μm were doped with Nile Red ($\lambda_{\text{abs}} = 532 \text{ nm}$, $\lambda_{\text{em}} = 590 \text{ nm}$) using a liquid two phase system described elsewhere [18]. Among the different techniques reported in the literature to either introduce a gain medium within a polymer microsphere [13] or simply coat its surface with either quantum dots or organic dye molecules [20,21], this approach enables high dye content to be attained within the polymer sphere which is critical for reaching the lasing threshold of the WGMs. Once the doping process complete, the sphere were rinsed by centrifugation, the supernatant removed and replaced by Millipore water.

2.3 Optical setup

To investigate the effect of positioning the resonator onto the tip of a suspended core MOF on the radiative modes of the resonator, we used the optical setup depicted in Fig. 1. An inverted microscope ($\times 100$ magnification) was modified for use in confocal mode, launching either a CW laser or a frequency-doubled YAG ($\sim 9 \text{ ns}$ pulse duration, 10Hz repetition rate) both emitting at $\lambda = 532 \text{ nm}$ through the microscope objective. In this configuration, the microscope was used for both the excitation and the collection of the fluorescence signal from the dye doped microspheres, using a dichroic mirror to filter out the excitation line. A monochromator (600, 1200 & 2400 l/mm) with a cooled CCD (2048 pixels) were used to record the WGM modulated fluorescence emission of the microsphere.

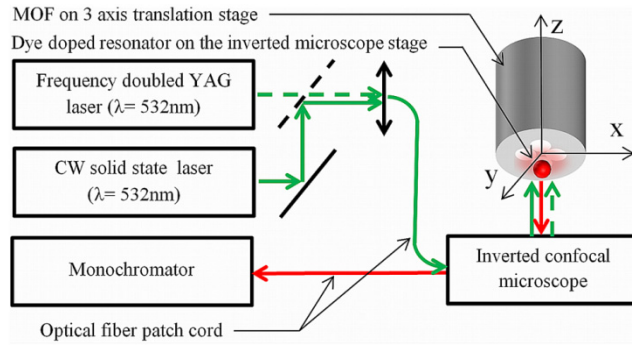


Fig. 1. Optical setup.

2.4 Microsphere attachment onto the MOF tip

An inverted microscope equipped with a second 3 axis translation stage was used in order to position the microsphere onto the silica MOF tip as shown in the Figs. 2(D) and 2(E). A drop of the free floating microsphere in Millipore water was deposited onto a glass cover slip and inspected using the inverted microscope while the freshly cleaved MOF was attached to the second translation stage with the fiber's tip pointing toward the drop of microsphere solution. A microsphere was selected from the many within the drop by qualitatively analyzing its emission spectrum via the confocal excitation and collection provided by the inverted microscope. Once located, the microsphere was put into contact with the tip of a 10 cm long MOF, which was aligned using the independent microscope stage. We believed that due to the hydrophobicity of both the polystyrene microsphere in water [22] and the presence of silanol groups (Si-OH) on the freshly cleaved silica MOF tip [23], once in contact, the microsphere tends to adhere to one of the holes of the MOF as shown in both Fig. 2(D) and 2(E).

3. Results and discussion

3.1 Characterization of the active resonator fluorescence emission

We initially selected microspheres from a batch with a diameter slightly larger than the effective hole diameter of the MOF (for the batch of fibers used here $\varnothing_{\text{hole}} \sim 17 \mu\text{m}$). As seen in Fig. 2(A), a periodic succession of 3 peaks is observed from the fluorescence emission of a 15 μm dye doped polystyrene microsphere, when this sphere is placed in contact with the glass slide or free floating in Millipore water and excited with the 532nm CW laser through the inverted confocal microscope. The two most intense peaks correspond to the different mode numbers of the first order modes with TE and TM polarization, while the least intense peak is attributed to higher order modes [4,24,25]. Once the same microsphere is then positioned onto the fiber tip, as shown in Figs. 2(D) and 2(E), the emission pattern of the sphere is significantly affected as can be seen in Fig. 2(A). As the holes of the MOF are not strictly circular, as it can be seen in the Fig. 2(D), the microsphere is never fully in contact with the inner surface of the MOF. The bright spot which could be seen in the Fig. 2(E) are due to the out coupling of the light from the microresonator induced by the fiber when they are in contact as describe later.

In both cases, the excitation power and collection efficiency remained the same as shown by the similar background level, since in this experiment the suspended core fiber is merely used to physically locate the resonator and break the refractive index symmetry around the resonator. While no light was guided through the fiber in this configuration and hence radiation changes cannot be attributed to the change of excitation efficiency due to the fiber, it nevertheless strongly impacted the emission of selected modes (depending on their polarization). For some cases, the intensity of the modes is enhanced by a factor of 8. This

enhancement is more pronounced for wavelengths between 610 nm and 620 nm, even though the maximum emission of the organic dye used to dope the sphere is around 590 nm. This can be explained by the significant decrease of the absorption of polystyrene from 590 to 620 nm as shown by Zhang et al. [26]. The analysis of the most intense resonance mode in both cases by fitting with a Gaussian function revealed an increase of the effective Q-factor ($Q = \lambda/\delta\lambda$) from 1170 for the free floating sphere, comparable to previously reported Q-factor in the literature for similar sphere size and material in water [25], to 1560 for the same sphere once attached to the MOF tip, resulting in a 33% increase. The WGM spectra before and after attachment to the MOF for larger microspheres, 20 μm and 25 μm in diameter, are shown in Figs. 2(B) and 2(C) respectively. While similar emission enhancement can be observed for the 20 μm sphere, it is far less pronounced and as the diameter mismatch between the sphere and the hole of the MOF increases it almost vanishes. From these results it becomes clear that the strongest enhancement is produced when the microsphere diameter matches the fiber's hole diameter, meaning that the microsphere sits lodged half way into the fiber hole. Note that in this configuration, the microsphere sees a ring of higher refractive index than its surrounding environment in a single equatorial plane.

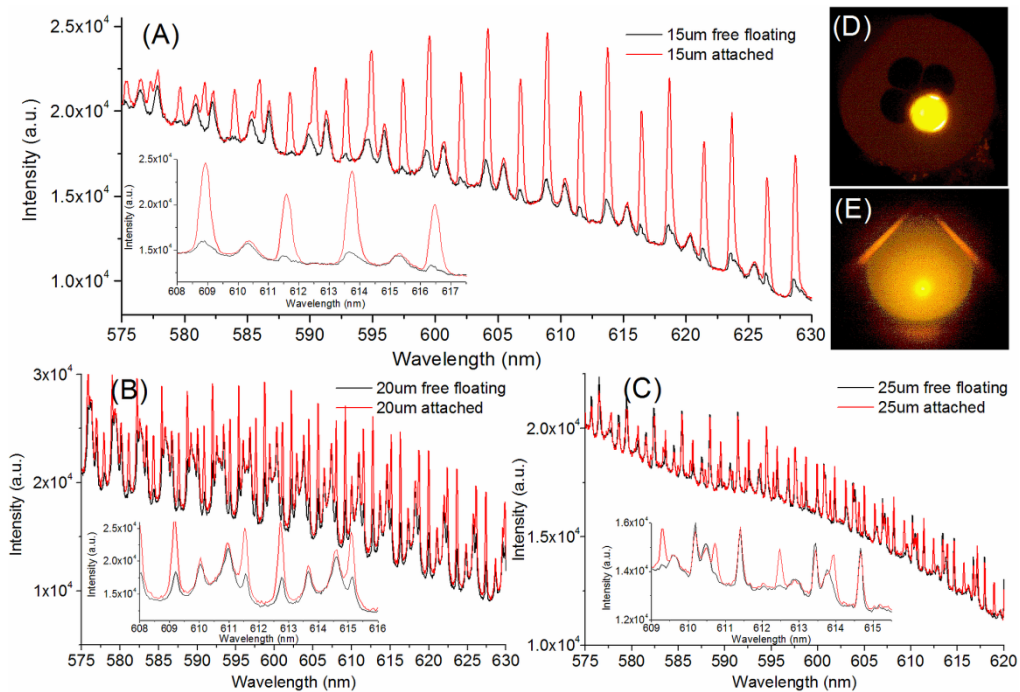


Fig. 2. Whispering gallery mode spectra of dye doped polystyrene microspheres with a nominal diameter of (A) 15 μm , (B) 20 μm and (C) 25 μm , free floating and positioned into a hole of a suspended core microstructured optical fiber ($\phi_{\text{hole}} = 17\mu\text{m}$). (D) and (E) are images of a fluorescing 15 μm polystyrene microsphere sitting onto the tip of the microstructured optical fiber.

3.2 Lasing behavior of the active resonator

The impact of the enhancement factor on the lasing properties of the WGMs is of particular interest in terms of its capacity to increase the Q-factor. Consequently, we repeated the experiment described above with the objective of evaluating the lasing threshold and efficiency as function of the mismatch between the resonator diameter and the MOF hole. To do this, we exchanged the CW laser source for a frequency-doubled YAG laser, delivering a 9ns pulse at a 10 Hz repetition rate.

Figure 3(A) shows two typical WGM spectra of another 15 μm dye doped polystyrene microsphere excited under the same condition below its lasing threshold, before (free floating) and after its attachment to the suspended core MOF (attached). As for the previous results with CW excitation, the active resonator exhibits mode enhancement when attached onto the fiber tip. Figure 3(B) shows the emission spectra of another 15 μm diameter polystyrene dye doped microsphere excited this time above its lasing threshold before (free floating) and after its attachment to the suspended core MOF (attached). As before, despite being excited at the same power the attached resonator again exhibits a higher intensity of its lasing mode. Figure 3(C) shows the amplitude of the lasing peaks of the same 15 μm resonator as a function of the pump power for the two different configurations (free-floating and attached resonator). In both cases, the microsphere fluorescence below the lasing threshold and the emission efficiency (slope) is increased above the lasing threshold. Both emission regimes have been fitted with a linear characteristic and the intersection of the fluorescence characteristic (dashed line) with the lasing characteristic (solid line) was used to determine the lasing threshold in both cases and we used the fitting error to determine the error on the lasing threshold. This yields a lasing threshold $P_{\text{threshold}} = 29 \pm 7 \mu\text{W}$ for the free-floating sphere and $P_{\text{threshold}} = 42 \pm 8 \mu\text{W}$ for the attached sphere. These values are comparable to previously reported lasing thresholds of similar dye doped resonators [17] and toroids [27]. Observe that the lasing threshold of the microsphere once attached is about 50% higher than the same microsphere free floating although it still falls within the same error margin which means that the difference of lasing threshold is not statistically significant. Nevertheless, we believe, as each microsphere was characterized first while freely moving in a liquid droplet prior a second characterization after being attached to the fiber tip, some of the dye molecules present within the resonator may have been photobleached while performing the first characterization, resulting in a decrease of the concentration of active dye and therefore a lower gain between the two successive characterizations. Similarly we analyzed the spectral position and linewidth of the resonance modes for one series of modes located around 611 nm which showed a similar pattern before and after being attached to the MOF tip. As the sphere operating above the lasing threshold clearly shows more resonances we had to use multiple Gaussian functions. Despite the difficulty of achieving a reliable fit in these conditions we found that for the free floating sphere the Q-factor is in the range of 6700, while the same sphere exhibits a Q-factor of up to 7700 for the same mode once attached to the fiber tip. More interesting is the comparison of the lasing efficiency in both cases. While the lasing efficiency for the free floating sphere is approximately $55 \pm 8 \text{ a.u./}\mu\text{W}$, the lasing efficiency of the same sphere once attached to the fiber reaches $490 \pm 12 \text{ a.u./}\mu\text{W}$, about 9 times higher. This lasing enhancement factor is in good agreement with the radiative enhancement factor observed under CW excitation. The same experiments were performed for $\varnothing = 25\mu\text{m}$ spheres. In this case, only a relatively modest enhancement of the lasing efficiency was observed (1.3 factor increase), while the lasing thresholds were comparable, $48 \pm 8 \mu\text{W}$ for the free floating sphere and $33 \pm 6 \mu\text{W}$ for the attached sphere.

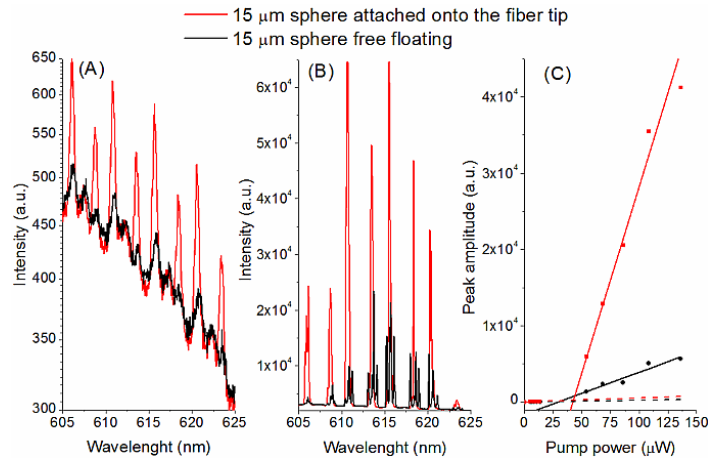


Fig. 3. (A) and (B) Whispering Gallery Mode spectra of a 15 μm dye doped polystyrene microsphere excited below and above lasing threshold respectively, before and after positioning onto the suspended core fiber. (C) Resonance intensity as function of the pump power for the same 15 μm dye doped polystyrene microsphere before and after positioning it onto the suspended core fiber tip.

3.3 Numerical modeling

To investigate the physical mechanism responsible for the experimentally observed peak enhancement, we employed a finite-difference time-domain (FDTD) analysis of a 2-dimensional approximation to the system. This geometry is shown in Fig. 4; the cross-section of the sphere is represented as an infinitely long cylinder of refractive index $n_p = 1.59$ (\approx polystyrene), embedded in a uniform solution of index $n_s = 1.333$ (\approx water). The rectangular blocks on either side represent the structure of a single hole of the MOF, imitating the contact points of the sphere with the MOF structure in the plane of interest. A plane collinear with the fiber axis (z direction in Fig. 1) is chosen as it is the likely plane of excitation and emission of the observed WGMs and best represents the experimental configuration in Fig. 1.

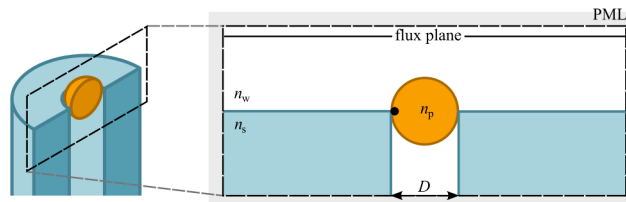


Fig. 4. Schematic diagram of the system and solution domain used in the 2D approximate numerical model, to relative scale. *Solid black line*: flux plane used to calculate the field's spectrum and power distribution. *Dashed boundary*: the edges of the simulation domain, surrounded by the perfectly matched layers required to eliminate artificial reflections of the radiated light. *Solid black circle*: position of the dipole source.

The calculations were performed with and without the presence of parallel blocks of index $n_g \approx 1.45$ (\approx silica) diametrically touching the circumference of the cylinder; as an approximation of the experimental configuration, as explained above. The diameter of the cylinder considered here is $D = 10 \mu\text{m}$, chosen to limit the required computational resources (which scale as D^2) while having a qualitatively similar behavior compared to larger D . Here we use the MIT *meep* package [28] as an FDTD solver. The solution domain is set to be $60 \mu\text{m}$ by $30 \mu\text{m}$ in size, centered about the cylinder, and terminated by perfectly matched layers (PMLs) of $2 \mu\text{m}$ thickness on the boundaries (Fig. 4). A dipole source is placed within the cylinder, 100 nm from the outer surface, to predominantly excite the resonant modes of

lowest radial order. Observation of the emitted radiation is emulated by placing a flux plane along the uppermost edge of the domain, where the glass blocks are placed on the lower portion of the domain, Fig. 4 (*top*), solid line. This simulates the situation of collecting the emitted light from a sphere via a microscope objective. The spectrum of the light transmitted across the full plane is calculated, as well as the spatial power distribution across the plane. The former is achieved by having the dipole radiate a Gaussian pulse with a spectrum centered at a wavelength of 600 nm and spectral width 40 nm (FWHM) in order to excite multiple azimuthal resonances, similar to the wide fluorescence spectrum of the dye doped microsphere demonstrated experimentally above.

The first result of note is the change in the radiated power distribution across the observation plane (integrated over all wavelengths), see Fig. 5. Compared to the power distribution of the resonator alone, the placement of glass blocks either side of the resonator has the effect of increasing the local power transmitted across the plane. The physical origins of this effect could include: a ‘lensing’ effect, where the high refractive index of the glass refracts the radiated light toward the center of the domain; increased out-coupling of light from the resonator due to the presence of the high-index medium, as exploited in prism-coupling of microresonators [4]; and scattering and reflection of the evanescent field at the water/glass interface. Indeed, this increase in observed local power could explain the ‘bright spots’ observed experimentally at the points where the microsphere touched the surrounding glass fiber as shown in the Fig. 2(E).

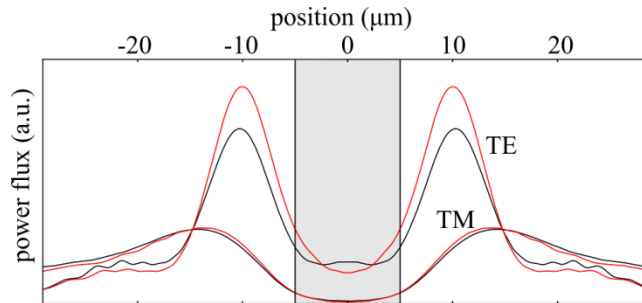


Fig. 5. *Top*: Calculated power distributions along the flux plane (Fig. 4) for TE (E_y) and TM (E_x) polarised sources (Fig. 6). *Black*: free standing resonator. *Red*: resonator surrounded by glass blocks (Fig. 4). Note the enhancement of the local radiated power for the TE light appearing to come from the contact points of the resonator and glass regions.

The model was further used to investigate changes in the WGM resonance spectra due to the presence of the glass blocks. Figure 6 shows the spectra of the light pulse collected along the entire flux plane, as per Fig. 4, in order to approximate the emission that would be collected by the microscope objective used in the experiments above. For both TE and TM polarization, the emission spectrum of the dipole is seen to be periodically modulated by discrete peaks due to the dipole coupling to the supported WGM resonances of the cylinder. The TE polarized dipole emission demonstrates a clear WGM peak enhancement upon addition of the glass blocks by almost a factor of 2. The TM polarization, however, appears almost unaltered by the change. These polarization dependent results are in qualitative agreement with the effects observed in experiment above. Two possible mechanisms for the observed resonance peak intensity enhancement are, firstly, a change in mode out-coupling (analogous to the power distribution change described above) and, secondly, an alteration of the dipole emission due to the change in the local environment. As for the polarization dependence, however, the authors believe its physical origin warrants further investigation as the effect in experiment is pronounced, the numerical simulations are in qualitative agreement, yet neither describe the mechanism itself. Similarly, note that in adding the high index structure about the resonator surface, the simulated TE resonance peaks are red-shifted

slightly (Fig. 6), as would be expected since the increase in surrounding index increases the effective optical path length of the WGMs, although this doesn't appear to be so for the TM polarization.

For free floating spherical resonators, it is reasonable to consider that the WGM spectral peaks are a superposition of resonance spectra from all contributing equatorial planes. Any asphericity will thus present a range of shifted resonances due to the various effective resonator diameters, broadening the peak. Enhancement of the radiation from a specific equatorial plane implies it would dominate the superposition, narrowing the peak. This would be observed as an effectively higher Q factor. As the modeling shows, such a plane of enhanced resonance emission should exist at the points where the sphere touches the glass fibre walls, *i.e.*, the 'bright spots' of Fig. 4. This is consistent with the experimental observation of the enhanced Q factor of the TE resonances in Sec. 3.2 (Fig. 3) and Sec. 3.4 (Fig. 7).

To bring the analysis closer to a quantitative description of the experiment, the model could be extended to include the simulation of a homogeneous emission layer rather than a point dipole source, the influence of higher order modes and the extension to a 3-dimensional domain in order to better describe the local coupling or scattering effects at the discrete contact points between the microsphere and fiber.

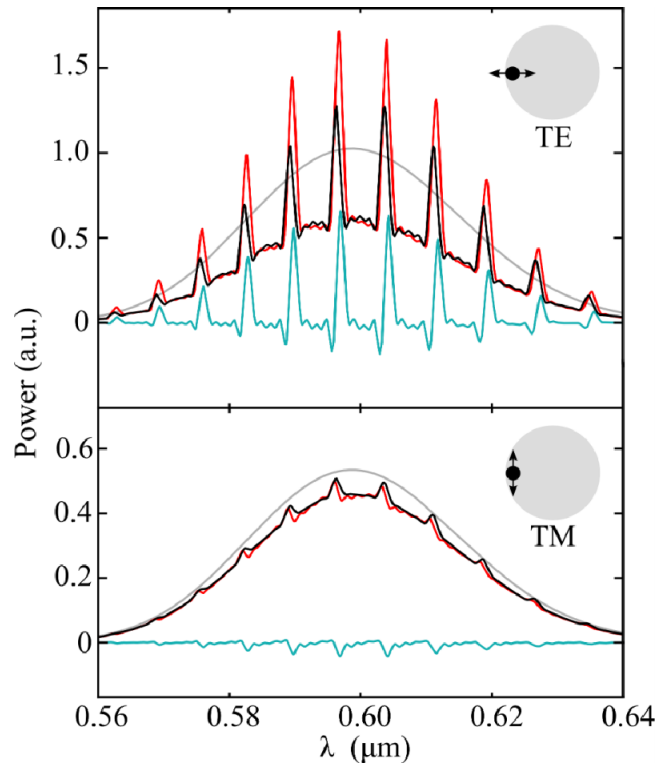


Fig. 6. Calculated spectra of the radiated fields from the cylinder described above (Fig. 4). *Grey line*: dipole source without cylinder or blocks. *Black*: cylinder without surrounding blocks. *Red*: cylinder with surrounding blocks. *Cyan*: difference of the black and red spectral lines, indicating alteration of the observed spectrum of the radiated light due to the presence of the adjacent high-index structure. *Top*: E_y , y -polarized dipole (TE polarization). *Bottom*: E_x , x -polarized dipole (TM polarization).

3.4 Pushing the limit of WGM sensing

While we have observed a significant enhancement of the emitted intensity of specific WGMs for a 15 μm microsphere, we sought to push this concept to its limit by tapering the suspended core fiber to enable a 5 μm microsphere to fit onto one of the tapered fiber's holes. The Fig. 7(A) shows the WGM spectra of dye doped polystyrene microspheres with a nominal diameter of 5 μm , both free floating and positioned into a hole of a tapered suspended core microstructured optical fiber ($\text{O}_{\text{hole}} \sim 5 \mu\text{m}$). Again, an enhancement of the modes can be clearly seen, although it seems that the enhancement factor does not depend on the polarization of the mode as strongly as for larger spheres. Furthermore, the enhancement factor is significantly smaller, by about a factor of 3 for both TE and TM modes, compared to the previous cases. We fitted the resonance modes with Gaussian functions to calculate the Q-factor as shown in the Figs. 7(B) and 7(C) for the same sphere free floating and after attachment to the tapered MOF tip respectively. The TE and TM modes of the free floating microsphere exhibit a Q-factor of 230 and 329 respectively, while the same modes for the same microsphere, once attached to the MOF tip, exhibit a Q-factor of 275 and 326. While the Q-factor of the TM mode considered remains constant, the Q-factor of the TE mode increases by 20%, following the trend predicted by the FDTD modeling. Nevertheless, Fig. 7(A) shows that positioning a sphere onto the tip of suspended core fiber turns an intrinsically poorly performing sphere into a usable sensor. The 20% increase of the effective Q-factor, directly related to the interaction between the resonator and the fiber, translates into higher resolution and therefore a better Detection Limit (DL) in terms of refractive index sensing.

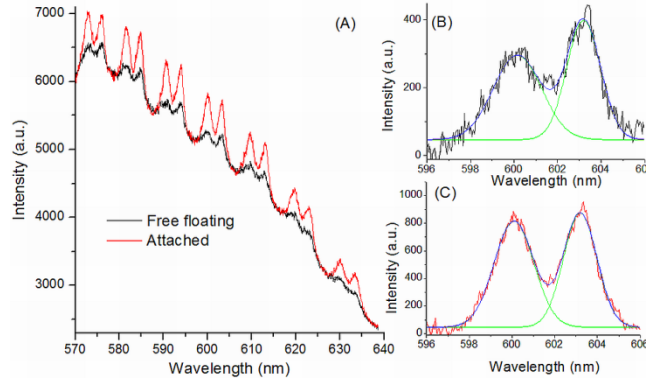


Fig. 7. (A) Whispering Gallery Mode spectra of dye doped polystyrene microspheres with a nominal diameter of 5 μm free floating and positioned into a hole of a tapered suspended core microstructured optical fiber ($\text{O}_{\text{hole}} \sim 5 \mu\text{m}$). (B) and (C) shows the details of the WGM spectra with a Gaussian fitting of the mode in the case of a free floating sphere and the same sphere once attached to the suspended core fiber, respectively

We evaluated the impact of the radiation enhancement on the detection limit using the formalism developed by White and Fan [29], where the Detection Limit (DL) is defined as the ratio between the sensor's Resolution (R) and its sensitivity (S) where $R = 3\sigma$, and where $R = 3\sigma$, and σ is the average noise contribution from the signal amplitude (σ_{Ampl}), the spectral position (σ_{Spectral}) and the thermal noise (σ_{Therm}) as described in Eq. (1) [29].

$$3\sigma = 3\sqrt{\sigma_{\text{Ampl}}^2 + \sigma_{\text{Spectral}}^2 + \sigma_{\text{Therm}}^2} \quad (1)$$

The noise on the signal amplitude σ_{Ampl} is defined by Eq. (2), the signal to noise ratio is defined by Eq. (3) and $\Delta\lambda$ the full width at half maximum of the WGM resonance ($Q = \Delta\lambda/\lambda$).

$$\sigma_{\text{Ampl}} = \frac{\Delta\lambda}{4.5(\text{SNR})^{0.25}} \quad (2)$$

$$\text{SNR} = 20 \times \log \left(\frac{\text{Signal Amplitude}}{\text{Noise Amplitude}} \right) \quad (3)$$

The signal to noise ratio (SNR) is defined in Eq. (3), where the noise amplitude on the resonance peak is defined as the standard deviation of the residual between a Gaussian fitting of the WGM peak and the experimental data and the signal amplitude is simply the signal intensity of the experimental data. In most cases, the SNR is close to 40dB.

For a rapid calculation of the other terms of the resolution, we kept the same value of σ_{Therm} used by White and Fan [29], while σ_{Spectral} was approximated to be limited by the linewidth of the resonance ($\sigma_{\text{Spectral}} = \lambda/100 \times Q$).

The results reported in the Table 1 show that the increase of radiation efficiency has in impact on both the amplitude noise (σ_{Ampl}) and the spectral noise (σ_{Spectral}). For the 15 μm sphere operated below their lasing threshold, the detection limit is improved from $\sim 4 \times 10^{-4}$ to $\sim 3 \times 10^{-4}$ RIU by simply fitting the hole diameter of the MOF with the resonator diameter. Once operated above their lasing threshold, the same trend can be observed with an improvement detection limit depending on whether the resonator is attached or not to the MOF tip. For the 5 μm polystyrene microsphere, the value of the detection limit is still smaller compared to the 15 μm microsphere despite the two fold increase of refractive index sensitivity.

Table 1. Theoretical calculations of the detection limit for different WGM sensor configurations.

	Q factor	Sensitivity (nm/RIU)	σ temp (nm)	σ spect (nm)	σ amp (nm)	DL (RIU)
15 μm free floating	1170	40	10×10^{-6}	5.30×10^{-3}	1.18×10^{-5}	3.97×10^{-4}
15 μm attached	1560	40	10×10^{-6}	3.97×10^{-3}	8.83×10^{-6}	2.98×10^{-4}
15 μm free floating lasing	6700	40	10×10^{-6}	9.25×10^{-4}	2.06×10^{-6}	6.94×10^{-5}
15 μm attached lasing	7700	40	10×10^{-6}	8.05×10^{-4}	1.79×10^{-6}	6.04×10^{-5}
5 μm floating	230	100	10×10^{-6}	2.70×10^{-2}	5.99×10^{-5}	8.09×10^{-4}
5 μm attached	329	100	10×10^{-6}	1.88×10^{-2}	4.19×10^{-5}	5.65×10^{-4}

This is mainly due to the intrinsically low Q factor of the smaller resonator which limits somehow the interest of using such a small sphere at this stage; this could be further improved by inducing lasing of this resonator or alternatively changing the material properties to reduce the absorption and scattering which limits the Q factor. Furthermore, the silica MOF used in this work do not present strictly circular hole which imply that a significant part of the sphere is not in contact with the inner surface of the fiber. We anticipate that using a specifically tailored MOF to exploit this phenomena, such as a hollow core fiber would result in an even higher enhancement of the radiation emission of the WGM and overall improved performances.

4. Conclusion

In conclusion, we have experimentally demonstrated that by positioning a dye-doped microsphere onto a hole at the cleaved tip of a suspended core MOF, it is possible to

significantly improve the radiation efficiency of the WGMs by a factor 8 and 9 below and above the lasing threshold, respectively. We investigated the dependence of this enhancement as a function of the diameter mismatch between the MOF hole and the sphere and found that the maximum enhancement is reached when the diameter of the resonator matches the MOF hole diameter where it sits, meaning that half the sphere protrudes into the MOF hole.

Qualitative agreement for the polarization dependent peak enhancement was found between the experimental results and FDTD numerical simulations, in which the system was approximated in 2 dimensions as a cylinder surrounded by glass blocks. Two effects were observed and discussed: an increase of the local power distribution in the observation plane and enhancement of the WGM peak spectral power.

We believe that this enhancement phenomenon will be extremely useful for biosensing applications for three reasons. Firstly, this phenomenon clearly results in both an increase of the signal-to-noise ratio of the radiation modes and the resonator's effective Q-factor. These two combined effects should enable higher resolutions to be reached, therefore improving the detection limit in terms of refractive index sensing. Secondly, we demonstrated that this effect can be exploited to use even smaller microspheres with higher sensitivity although further work is required to take full advantage of the higher refractive index sensitivity and compensate the spoiling of the Q factor.

Acknowledgments

T. Monro acknowledges the support of an ARC Federation Fellowship as well as the support of DSTO Australia. K. Rowland acknowledges the support of an ARC Super Science Fellowship. This work was performed in part at the Optofab node of the Australian National Fabrication Facility, a company established under the National Collaborative Research Infrastructure Strategy to provide nano and microfabrication facilities for Australia's researchers.